Final Draft

of the original manuscript

Gleißner, R.; Beck, E.E.; Chung, S.; Semione, G.D.L.; Mukharamova, N.; Gizer, G.; Pistidda, C.; Renner, D.; Noei, H.; Vonk, V.; Stierle, A.:

Operando reaction cell for high energy surface sensitive x-ray diffraction and reflectometry.

In: Review of Scientific Instruments. Vol. 93 (2022) 7, 073902.

First published online by AIP: 07.09.2021

https://dx.doi.org/10.1063/5.0098893

Operando Reaction Cell for High Energy Surface Sensitive X-ray Diffraction and Reflectrometry

R. Gleißner,[1,2] E. E. Beck,[1,2] Simon Chung,[1] G. D. L. Semione,[1,2,a)] N. Mukharamova,[1] G. Gizer,[3] C. Pistidda,[3] D. Renner,[1] H. Noei,[1] V. Vonk,[1] and A. Stierle[1,2]

[1)] *Centre for X-ray and Nano Science CXNS, Deutsches Elektronen-Synchrotron DESY, Notkestraße 85, 22607 Hamburg, Germany*

[2)] *Fachbereich Physik, Universität Hamburg, Jungiusstraße 9, 20355 Hamburg, Germany.*

[3)] *Institute of Hydrogen Technology, Materials Technology, Helmholtz-Zentrum hereon GmbH, Max-Planck-Straße 1, 21502 Geesthacht, Germany*

(*Electronic mail: andreas.stierle@desy.de)

(Dated: 15 June 2022)

A proof of concept is shown for the design of a high pressure heterogeneous catalysis reaction cell suitable for surface sensitive X-ray diffraction and X-ray reflectometry over planar samples using high energy synchrotron radiation in combination with mass spectrometry. This design enables measurements in a pressure range from several tens to hundreds of bars for surface investigations under realistic industrial conditions in heterogeneous catalysis or gaseous corrosion studies.

I. INTRODUCTION

Over the last decades, the development of machinery that combines the advantages of traditional surface science methods and operando reaction conditions advanced rapidly. Tools like e.g. ambient pressure X-ray photoelectron spectroscopy[1,2] and ambient pressure scanning tunneling microscopy[3–5] demonstrated in a variety of successful experiments that it is possible to achieve an atomistic understanding of the contributing surfaces and reaction mechanics in non-vacuum conditions. Hard X-ray scattering can also address the surface structure, is not hindered by non-vacuum conditions and can penetrate chamber walls[6]. Several sample environments have been developed for surface sensitive X-ray diffraction[7,8] or high pressure X-ray reflectivity[9–11]. In many cases the industrially relevant reaction pressures can be several orders of magnitude higher than ambient pressure, e.g. the synthesis of methanol and hydrogenation of CO_2 over $Cu/ZnO/Al_2O_3$ catalysts utilizes temperatures of 470–520 K and pressures of 50 bar and above in industrial plants[12]. In order to completely overcome the pressure gap between ultra high vacuum and realistic reaction conditions for surface science investigations, especially for catalysis under gas flow, new instruments need to be created.

Fixed-bed cells utilizing powder samples have previously been designed for the use of X-ray absorption spectroscopy and X-ray diffraction measurements to obtain information of the structure of the catalyst while simultaneously probing the gas environment under operando conditions[13–18]. While certain knowledge can be extracted from powder diffraction experiments, surface sensitive X-ray diffraction is a more elaborate tool and better suited to achieve a detailed understanding of the catalysts surface interactions[19]. It utilizes single crystalline samples that can be covered with nanoparticles, adlayers or be otherwise conditioned to mimic a specific catalytic interplay[7]. Information about surface roughness, surface reconstruction effects, defects as well as the strain, size, orientation and lattice spacing of the nanoparticles or adlayers can be acquired for the specific single crystal facet under investigation[7]. Additionally, x-ray reflectrometry can be performed in this measurement geometry, which yields information about the layer thickness, interface roughness and the electron density profile at the surface, e.g. nanoparticle height and surface coverage.

A variety of advancements in the combination of surface sensitive X-ray diffraction with other experimental methods were developed in the last decades such as ellipsometry[20], X-ray photoelectron spectrometry[21], surface optical reflectance and planar laser induced fluorescence[22] or the use of electrochemically integrated flow cells[23], pioneering an intertwined understanding from different points of view.

In this article, we present the design of a high pressure operando reaction cell for high energy surface sensitive X-ray diffraction (HE-SXRD) and X-ray reflectometry (XRR) on single crystalline samples and supported nanoparticles. Measurements were performed utilizing pressures up to 50 bar of Ar, H_2, CO and CO_2 with sample temperatures up to 600 K. While the pressure and temperature limits of the capillary itself were not tested in this proof-of-concept study, similar cell geometries point toward pressure ranges up to several hundred bars[24].

II. SETUP DESIGN

The main concept of the instrument is based on a single crystalline Al_2O_3 capillary, which acts both as the gas pressure cell and the window for the hard X-rays. This material was chosen as it has proven to withstand pressures of up to 700 bar at 770 K[24] and is sufficiently transmissive for a high energy synchrotron beam with e.g. $h\nu = 73$ keV (see Figure 1). With the utilized cell geometry, the X-ray beam passes through 1 mm Al_2O_3 twice as incident beam and after reflec-

[a)] Current address:University of Bremen, MAPEX Core Facility for Materials Analytics, MAPEX Center for Materials and Processes, 28334, Bremen, Germany.

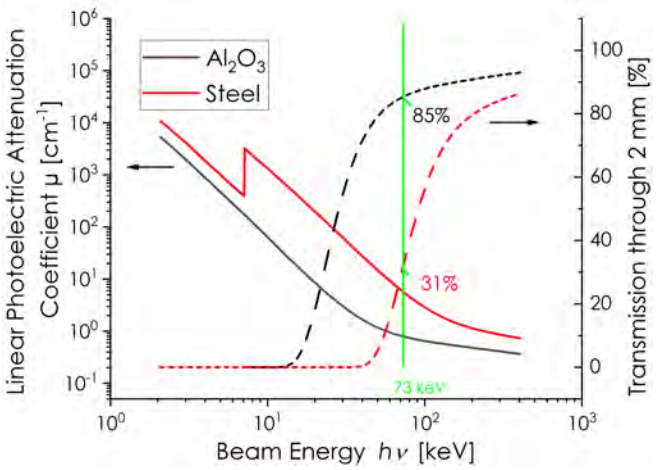

FIG. 1. The linear photoelectric X-ray attenuation coefficient μ (left axis)[25] and transmission I/I_0 through 2 mm material (right axis) of Al_2O_3 (black) as utilized for the experimental reaction cell compared to steel ($Fe_{99}C_1$, red).

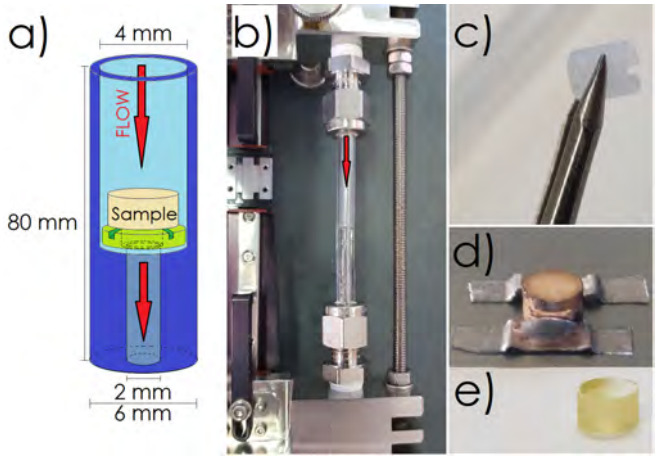

FIG. 2. Reaction cell design. a) Scheme of the capillary with two inner diameters of 2 mm and 4 mm, the crown spacer (green) and the single crystal sample. b) Reaction cell mounted in holding stage. c) Al_2O_3 crown spacer in detail. Cylindrical Cu (d) and ZnO (e) samples of 3.5 mm diameter.

tion/diffraction from the sample, loosing 15% of its intensity due to absorption and scattering with the capillary. The usage of e.g. steel as capillary material would decrease the X-ray transmission through the cell significantly for photon energies below 100 keV and would furthermore lead to a high number of artifacts originating from its polycrystalline domains. Rather than utilizing an amorphous or polycrystalline cell material which increases the overall background in the detector images, the goal is to identify and individually block the Bragg peaks that are diffracted off the single crystalline capillary. Another important advantage is the low thermal conductivity of oxide-based capillaries compared to metals, which enables the use of polymer ferrules as gaskets of the capillary during measurements at elevated temperatures.

Reaction Cell

The experiment design features three assemblies: the gas supply system, the reaction cell assembly as well as the pressure regulator and gas analysis section. They are separated by flexible tubing that allows the reaction cell assembly to be mounted on a tower of goniometers and linear translators. The reaction cell itself consists of a single crystalline Al_2O_3 capillary with two inner diameters of 2 mm and 4 mm, intersecting at the center of the capillaries' full length (Figure 2a). Thus, an edge is presented where a round Al_2O_3 'crown spacer' (Figure 2c) is introduced through the larger opening. It serves three purposes, as it 1) directs the gas flow around the sample, preventing the capillary to be clogged, 2) accounts for the transition angle at the intersection of the two inner diameters with a phase at the bottom of the crown spacer, which prevents rocking motions during the measurements and 3) is an inexpensive and exchangeable part to easily tune the height of the sample inside the reaction cell. This height is of importance, as the Al_2O_3 capillary usually has at the intersection of the two inner diameters a higher impurity density, polycrystallinity and other defects due to the manufacturing process. Crown spacer and sample are introduced into the capillary by sliding them subsequently onto the internal step prior to mounting the capillary into the holding stage. The sample was found to be placed sufficiently stable for all necessary angular and translational movements of the goniometer stage in a grazing incidence beam geometry, as the gas flow additionally presses sample and crown spacer against the internal capillary step. The sample geometry requires a diameter D_S and height H_S that fulfills $\sqrt{H_S^2 + D_S^2} > D_C$ with D_C being the larger inner diameter of the capillary in order to avoid flipping of the sample to its side. A minimum height H_S of 1.0 mm for metal and 1.5 mm for oxide samples is recommended if side slits are used for mounting in e.g. UHV systems in order to avoid bending or breaking of the sample surface.

For the connection to the gas supply, Vespel® ferrules are utilized to seal against the hot, high pressure, potentially corrosive and toxic gas feed. The top and bottom connections (Figure 2b) can be linearly translated to adjust for different capillary lengths and for capillary mounting purposes. The rigidity of the frame against the high pressures is ensured by connection screws (right side) which are affixed after the mounting of the capillary. An excess flow valve upstream and a check valve downstream from the capillary shut off the gas supply in case of capillary rupture.

A thermocouple can be introduced from the bottom of the capillary frame through a Vespel ferrule sealed feedthrough, upwards inside the 2 mm inner diameter of the capillary contacting the backside of the sample. If the sample is metallic, the thermocouple could be welded directly to the sample to allow for temperature measurement during the experiment. For insulating samples, it would be recommended to run a temperature calibration prior to the experiment, as the thermocouple may loose contact during heating.

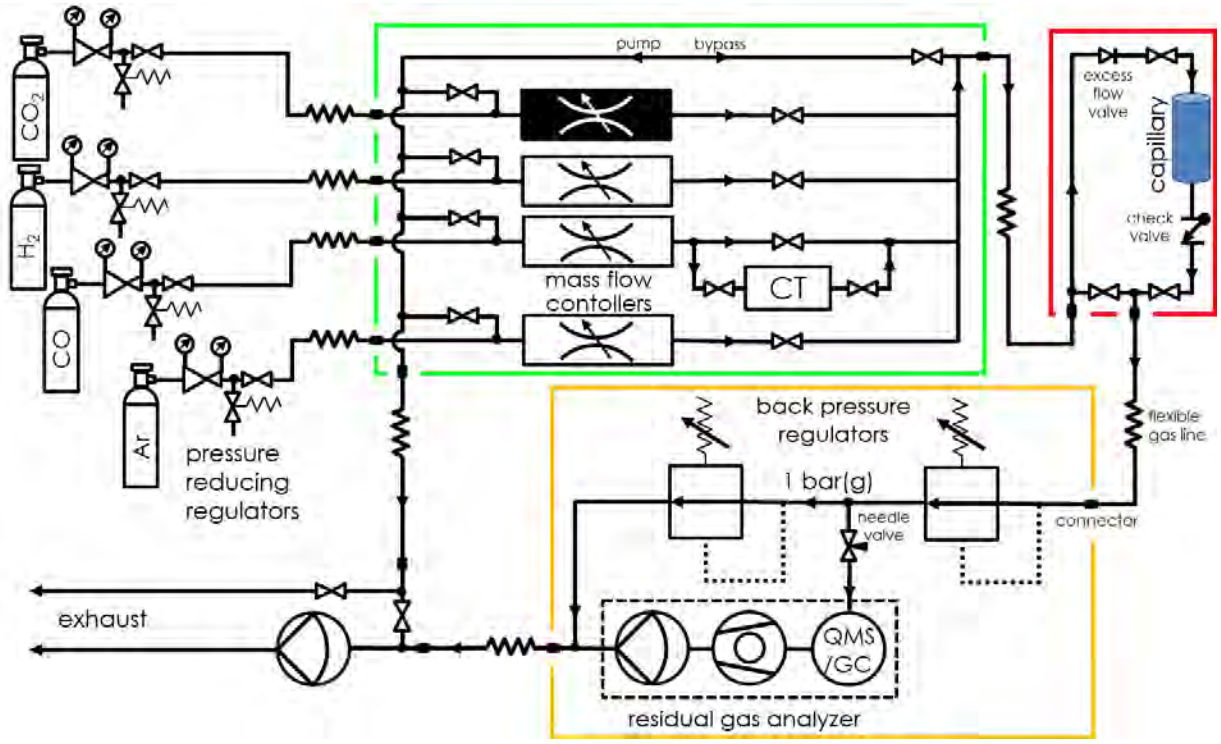

FIG. 3. Technical scheme of the gas handling system (green square), the reaction cell assembly (red square) as well as the pressure regulator and gas analysis section (orange square) of the high pressure HE-SXRD experimental setup.

Gas Supply System and Gas Analysis

Figure 3 depicts the technical scheme of the gas handling system. In this configuration, it utilizes H_2, Ar, CO, and CO_2 as feed gases as used in a wide variety of experiments e.g. the water gas shift reaction, methanol or Fischer-Tropsch synthesis.

The Ar, H_2 and CO gas lines feature mass flow controllers (Bronkhorst® EL-FLOW Select) while the CO_2 line utilizes a Coriolis mass flow controller (Bronkhorst® mini CORI-FLOW) as required by the low condensation pressure of about 50 bar at room temperature (triple point at 31.0 °C and 73.9 bar). For precise operation, the latter must be mounted on a vibration suppressing stand. The CO gas supply requires the use of a carbonyl trap (CT; PALL Mini GasKleen®) for which we utilized an active material gas purifier. It is important to note that the carbonyl trap should be mounted upstream from the H_2 and CO_2 supply lines to avoid degradation of its active material. Two back pressure regulators (BPR; Bronkhorst® EL-PRESS) keep the reaction cell at the desired experimental pressure while regulating the pressure in between them to 1 bar(g), from which a sample gas stream is leaked trough a needle valve into the quadrupole mass spectrometer (QMS) or gas chromatograph (GC). For mass spectrometry, long dwell times of the gas feed on the sample surface are needed to account for the small surface area of single crystals compared to powder samples. Thus, a flow rate range of 0.9-45 ml(n)/min for each individual mass flow controller was chosen. The operation of the utilized mass flow controllers requires differential pressures of minimum 13 bar(g) and maximum 40 bar(g). Thus, for pressures above 40 bar(g) either a step wise increase of the inlet and outlet pressure or a pre-pressurization from the bypass gas supply is needed.

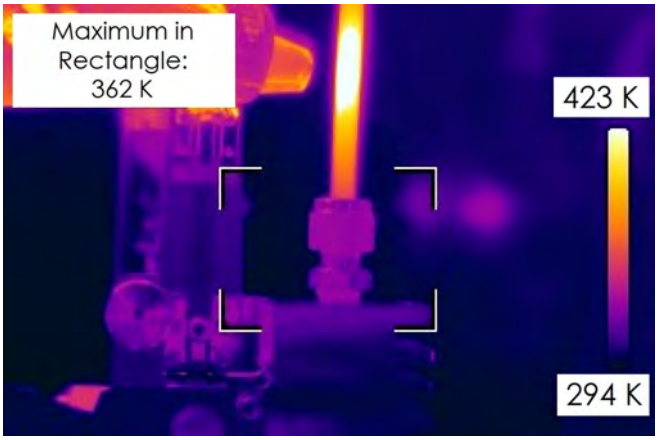

FIG. 4. Infra red camera image of the capillary with a heat gun temperature of $T_{gun} = 820$ K and 50 bar Ar at 45 ml(n)/min, achieving a sample temperature of 575 K.

Bypasses and a vacuum pump were integrated to evacuate and flush all gas lines in order to remove contamination and residual moisture. Depressurization to about ambient pressures via a gradual relief valve bypassing the pump is necessary prior to its operation.

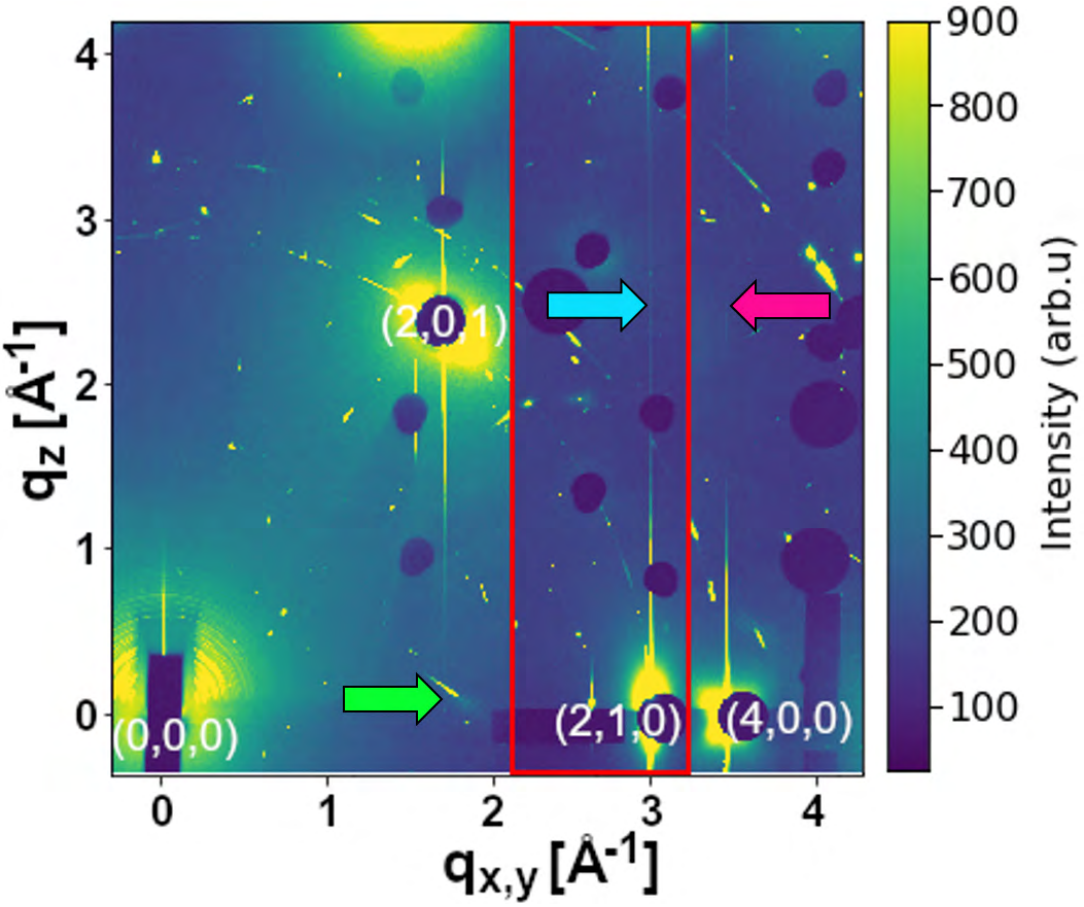

FIG. 5. High energy surface sensitive X-ray diffraction measurement of a Cu(110) surface at room temperature and 30 bar H_2 after heating to 520 K under 30 bar H_2 displayed in reciprocal space. The image shows the maximum pixel intensity over a range of $\omega = 20°$ around the (2,0) and (4,0) CTRs as well as around the (2,1) CTR (red outlined inset). White labels indicate the Cu Bragg peaks in surface coordinates[26]. An X-ray photon energy of $h\nu = 67$ keV with a grazing incidence angle of $\theta_i = 0.06°$ at 3.4 keV bandwidth and a Varex Imaging XRD 4343CT detector[27] were utilized. The green, magenta and cyan arrows point at CTR intensity minima for which line scans are depicted in Figure 6.

Heating and Temperature

To increase the sample temperature to the desired experimental conditions, an external heat gun is utilized that directs a flow of hot air onto the capillary. In this proof-of-concept, a Steinel® HG 2320E heat gun with an attached metal cone to focus the air flux was used, which was able to deliver hot air between 350 K and 920 K with an air flux of 150 or 500 L/min. It should be freestanding and not mounted attached to the diffraction setup in order to to avoid blockage of the X-ray beam pathway. The temperature of the sample is rather influenced by the geometry of the heat gun setup than by changes of the flow rate or pressure of the gas feed inside the capillary. Thermal expansion effects that lead to misalignment of the sample surface with respect to the X-ray beam are easy to adjust for, though significant compared to the narrow beam sizes of typically 2–3 μm for high energy grazing incidence XRD experiments[28].

The length of the capillary plays an important role in the safety concept of the experimental cell, as the Vespel ferrules exhibit a maximum operation temperature of 620 K. In order to achieve sample temperatures of 600 K and beyond, the Al_2O_3 capillary surpasses the maximum operation temperature of the ferrules at the height of the sample. With a distance of 4 cm to the ferrules, the low thermal conductivity[29] of the Al_2O_3 capillary of 50 $W \cdot m^{-1} \cdot K^{-1}$ and the heat exchange with the gas inside and outside of the capillary is sufficient enough to achieve temperatures within the operation limits of the ferrules, as seen in Figure 4.

III. EXAMPLE MEASUREMENTS

Figure 5 displays high energy X-ray diffraction data of a Cu(110) single crystal at room temperature and 30 bar H_2 after heating to 520 K under 30 bar H_2. Figure 6 depicts $\Delta q_{x,y}$ scans in reciprocal space horizontally across the minima of the three crystal truncation rods (CTRs)[30,31] shown in Figure 5. The acquisition of signal data at these points in reciprocal space serves as a proof of concept that the designed reaction cell is suitable for these kind of measurements. The presence of the signal indicates that the Cu(110) surface stays atomically

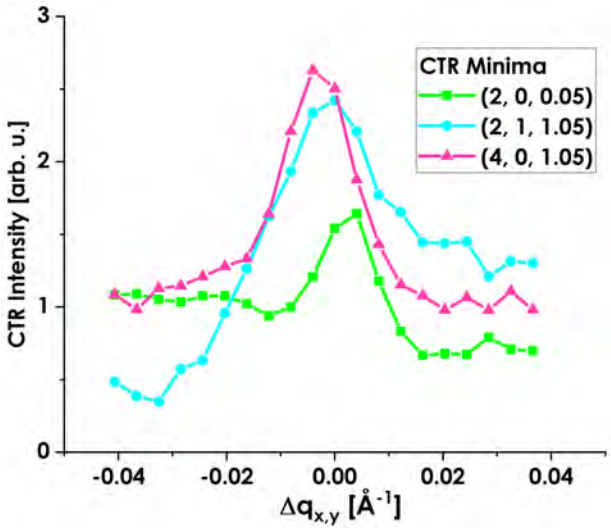

FIG. 6. $\Delta q_{x,y}$ line scans in reciprocal space horizontally across the CTRs of the Cu(110) sample at 30 bar H_2 and room temperature. The coordinates in the legend correspond to h, k, l values in Cu(110) surface coordinates as depicted in Figure 5. The line scans were chosen at $l = 0.05$ and $l = 1.05$ to accommodate for the influence of the sample horizon as well as signals originating from layer occupation factors of the surface atoms that result in a local maximum at integer values of l.

smooth at 30 bar H_2 exposure.

Besides the Cu CTRs on the detector, numerous intense artifacts are visible that arise from the Al_2O_3 capillary. The 'random' placement of these features arise due to to the transmission twice through the Al_2O_3 capillary wall, although it also indicates that the capillary was fairly polycrystalline at the height of the sample surface. We are confident that the observed artifacts in the HE-GIXRD images can be largely reduced by the use of a capillary of higher quality, i.e. larger grain sizes to a point where they can be individually blocked by beam stops on the 2D detector. Since the unsatisfying quality is a result of the fusing process of two separate capillaries, this may be circumvented by alternatively boring holes with 2 mm and 4 mm inner diameter into a solid Al_2O_3 cylinder. In addition, the use of a higher crown spacer can offset the samples' surface away from the capillary region of poor quality.

IV. CONCLUSIONS

This study shows a proof-of-concept for a operando reaction cell for surface sensitive high-energy grazing-incidence X-ray diffraction and reflectometry utilizing single crystal samples or samples with mirror like surfaces. The test measurements were performed up to a maximum of 50 bar Ar and a sample temperature of 600 K, yet higher values are expected to be achievable. The use of a gas supply system allows for the use of gas feeds containing mixtures of Ar, H_2, CO and CO_2. Once capillaries of satisfying crystal quality have been obtained, stability stress tests will reveal which catalytic systems, reactions or surface mechanisms of interest come into question to be studied in this conceptional setup. First experiments demonstrate that the surface signal from a Cu(110) single crystal at 30 bar H_2 pressure can be extracted, despite the high background from the capillary. As the operational range of surface science techniques extends to several tens to hundreds of bars, surface studies of model systems under true industrial conditions become feasible.

CONFLICTS OF INTERESTS

The authors have no conflicts to disclose.

ACKNOWLEDGMENTS

We acknowledge DESY (Hamburg, Germany), a member of the Helmholtz Association HGF, for the provision of experimental facilities. Parts of this research were carried out at PETRA III, P21 beamline. We acknowledge support by the Helmholtz Foundation through the Helmholtz-Lund International Graduate School (HELIOS, HIRS-0018). We also thank the Helmholtz Energy Materials Characterization platform (HEMCP) for instrumental support.

DATA AVAILABILITY STATEMENT

Raw data were generated at the PETRA III beamline P21.2 at DESY (Hamburg, Germany). Derived data supporting the findings of this study are available from the corresponding author upon reasonable request.

[1] M. Salmeron, Topics in Catalysis **61**, 2044 (2018).
[2] C. Schlueter, A. Gloskovskii, K. Ederer, I. Schostak, S. Piec, I. Sarkar, Y. Matveyev, P. Lömker, M. Sing, R. Claessen, C. Wiemann, C. M. Schneider, K. Medjanik, G. Schönhense, P. Amann, A. Nilsson, and W. Drube, in *AIP Conference Proceedings*, Vol. 2054 (2019) pp. 040010–040016.
[3] F. Tao, L. Nguyen, and S. Zhang, Review of Scientific Instruments **84**, 034101 (2013).
[4] R. V. Mom, W. G. Onderwaater, M. J. Rost, M. Jankowski, S. Wenzel, L. Jacobse, P. F. Alkemade, V. Vandalon, M. A. van Spronsen, M. van Weeren, *et al.*, Ultramicroscopy **182**, 233 (2017).
[5] C. Herbschleb, P. Van Der Tuijn, S. Roobol, V. Navarro, J. Bakker, Q. Liu, D. Stoltz, M. Cañas-Ventura, G. Verdoes, M. Van Spronsen, *et al.*, Review of Scientific Instruments **85**, 083703 (2014).
[6] V. Vonk and H. Graafsma, in *In-situ Materials Characterization* (Springer, 2014) pp. 39–58.
[7] A. Stierle, J. Gustafson, and E. Lundgren, in *Operando Research in Heterogeneous Catalysis* (Springer, 2017) pp. 59–87.
[8] P. Bernard, K. Peters, J. Alvarez, and S. Ferrer, Review of scientific instruments **70**, 1478 (1999).
[9] F. J. Wirkert, M. Paulus, J. Nase, J. Möller, S. Kujawski, C. Sternemann, and M. Tolan, Journal of synchrotron radiation **21**, 76 (2014).
[10] F. Venturini, S. Schöder, W. F. Kuhs, V. Honkimäki, L. Melesi, H. Reichert, H. Schober, and F. Thomas, Journal of synchrotron radiation **18**, 251 (2011).
[11] A. de Jong, V. Vonk, V. Honkimäki, B. Gorges, H. Vitoux, and E. Vlieg, Journal of Crystal Growth **420**, 84 (2015).
[12] M. Bowker, ChemCatChem **11**, 4238 (2019).
[13] S. K. Matam, M. Aguirre, A. Weidenkaff, and D. Ferri, The Journal of Physical Chemistry C **114**, 9439 (2010).

[14]B. A. Talagañis, F. Castro, A. Baruj, and G. Meyer, Review of Scientific Instruments **80**, 073901 (2009).
[15]B. R. S. Hansen, K. T. Møller, M. Paskevicius, A.-C. Dippel, P. Walter, C. J. Webb, C. Pistidda, N. Bergemann, M. Dornheim, T. Klassen, J.-E. Jørgensen, and T. R. Jensen, Journal of Applied Crystallography **48**, 1234 (2015).
[16]U. Bösenberg, C. Pistidda, M. Tolkiehn, N. Busch, I. Saldan, K. Suarez-Alcantara, A. Arendarska, T. Klassen, and M. Dornheim, International Journal of Hydrogen Energy **39**, 9899 (2014).
[17]B. Clausen, Journal of Catalysis **132**, 524 (1991).
[18]P. J. Chupas, K. W. Chapman, C. Kurtz, J. C. Hanson, P. L. Lee, and C. P. Grey, Journal of Applied Crystallography **41**, 822 (2008).
[19]U. Hejral, D. Franz, S. Volkov, S. Francoual, J. Strempfer, and A. Stierle, Physical review letters **120**, 126101 (2018).
[20]S. Couet, T. Diederich, K. Schlage, and R. Röhlsberger, Review of Scientific Instruments **79**, 093908 (2008).
[21]G. Eres, C. M. Rouleau, Q. Lu, Z. Zhang, E. Benda, H. N. Lee, J. Z. Tischler, and D. D. Fong, Review of Scientific Instruments **90**, 093902 (2019).
[22]S. Pfaff, J. Zhou, U. Hejral, J. Gustafson, M. Shipilin, S. Albertin, S. Blomberg, O. Gutowski, A. Dippel, E. Lundgren, *et al.*, Review of Scientific Instruments **90**, 033703 (2019).
[23]D. Burkle, R. De Motte, W. Taleb, A. Kleppe, T. Comyn, S. Vargas, A. Neville, and R. Barker, Review of Scientific Instruments **87**, 105125 (2016).
[24]N. Aslan, C. Horstmann, O. Metz, O. Kotlyar, M. Dornheim, C. Pistidda, S. Busch, W. Lohstroh, M. Müller, and K. Pranzas, Journal of Neutron Research **21**, 125 (2019).
[25]C. Chantler, K. Olsen, R. Dragoset, J. Chang, A. Kishore, S. Kotochigova, and D. Zucker, "X-Ray Form Factor, Attenuation and Scattering Tables — NIST Standard Reference Database 66," (2005), date of Access: 6th of October, 2021.
[26]T. P. Trainor, P. J. Eng, and I. K. Robinson, Journal of applied crystallography **35**, 696 (2002).
[27]*Varex Imaging XRD 4343CT Industrial Flat Panel Detector*, ©2021 Varex Imaging Corporation, https://www.vareximaging.com/wp-content/uploads/2022/01/XRD-4343CT_118914-1.pdf (accessed: 24.04.2022).
[28]H. Reichert, V. Honkimäki, A. Snigirev, S. Engemann, and H. Dosch, Physica B: Condensed Matter **336**, 46 (2003).
[29]K. E. Petersen, Proceedings of the IEEE **70**, 420 (1982).
[30]I. K. Robinson, Phys. Rev. B **33**, 3830 (1986).
[31]U. Hejral, P. Müller, M. Shipilin, J. Gustafson, D. Franz, R. Shayduk, U. Rütt, C. Zhang, L. Merte, E. Lundgren, *et al.*, Physical Review B **96**, 195433 (2017).